Author Manuscript

Geomagnetic Disturbances due to Neutral-wind-driven Ionospheric Currents

Cheng Sheng[1], Yue Deng[1], Daniel T. Welling[1,2], and Steven K. Morley[3]

[1]Department of Physics, University of Texas at Arlington, Arlington, Texas, USA

[2]Department of Climate & Space, University of Michigan, Ann Arbor, Michigan, USA

[3]Space Science and Applications, Los Alamos National Laboratory, Los Alamos, NM, USA

Corresponding author: Yue Deng (yuedeng@uta.edu)

Key Points:

1. Neutral-wind-driven currents contribute to about 10-30% of the total geomagnetic disturbances (GMDs) at locations where the high-latitude electric potential is dominant.
2. During the storm recovery phase, neutral-wind-driven currents are the primary sources for middle-latitude GMDs on the dayside.
3. At middle latitudes, the magnitude of recovery-time neutral-wind-driven GMDs is comparable to that caused by ring currents.

This is the author manuscript accepted for publication and has undergone full peer review but has not been through the copyediting, typesetting, pagination and proofreading process, which may lead to differences between this version and the Version of Record. Please cite this article as doi: 10.1029/2023SW003750.

This article is protected by copyright. All rights reserved.

Author Manuscript

Abstract

Previous simulation efforts on geomagnetic disturbances (GMDs) and geomagnetically induced currents (GICs) mostly rely on global MHD models, which explicitly calculate the magnetospheric currents and carry certain assumptions about the ionosphere currents. Therefore, the role of ionospheric and thermospheric processes to GMDs has not been fully evaluated. In this study, Global Ionosphere Thermosphere Model (GITM) simulations for an idealized storm event have been conducted. Simply, the high-latitude electrodynamic forcing (potential pattern and particle precipitation) has been specified by empirical models. GMDs due to neutral-wind driven currents have been compared to those caused by magnetospheric convection driven currents during both the main and recovery phases. At locations where the high-latitude electric potential is dominant, neutral-wind driven currents are found to contribute to about 10-30% of the total GMDs. During the recovery phase when the ion-convection pattern retreats to high latitudes, neutral-wind driven currents become the primary sources for GMDs at middle latitudes on the dayside due to the "flywheel" effect and the large dayside conductance. Our result strongly suggests that ionospheric and thermospheric processes should not be neglected when estimating GMDs and therefore GICs.

Plain Language Summary

Disturbances of magnetospheric and ionospheric current systems in the near-Earth environment can induce strong geomagnetic disturbances (GMDs) and geomagnetically induced currents (GICs) at the ground level and then cause serious damage to important infrastructures, such as power grids and pipelines. Previous studies used magnetohydrodynamics (MHD) models to explicitly calculate the current system in the magnetosphere and used empirical formulas to estimate the current system in the ionosphere. Such approach simplifies the ionospheric and

This article is protected by copyright. All rights reserved.

thermospheric processes and their contribution to the ionospheric current system. In this study, an ionosphere-thermosphere model is used to simulate the ionospheric current system during an idealized event, and the main objective is to evaluate the importance of neutral-wind-driven currents. It is found that during the storm recovery phase, neutral-wind-driven currents are the primary sources for middle-latitude GMDs on the dayside.

Author Manuscript

This article is protected by copyright. All rights reserved.

1. Introduction

Geomagnetic disturbances (GMDs or ΔB) and geomagnetically induced currents (GICs), which are manifestations of space weather impacts at the ground level, pose a serious threat to the reliability of important infrastructures, such as power grids and pipelines, especially during intense geomagnetic storms [e.g, *Boteler.*, 2001; Gummow and Eng, 2002; Ngwira and Pulkkinen, 2019]. The sources of GMDs and GICs are disturbances of magnetospheric and ionospheric current systems in the near-Earth environment. These current systems are the result of a combination of solar drivers and internal system dynamics. Global magnetohydrodynamic (MHD) models, coupled with height-integrated ionospheric electrodynamic models, are usually used for GMD and GIC simulations and predictions [Welling, 2019]. The coupled models calculate magnetospheric currents explicitly and estimate ionospheric conductance by using empirical formulas [*Welling et al.*, 2017]. For example, the *Robinson et al.* [1987] formulas are usually used to estimate the ionospheric conductance from the average energy and energy flux of precipitating electrons at high latitudes. Such an approach with MHD models may oversimply the 3-dimensional ionospheric currents as well as the ionospheric and thermospheric processes that contribute to the ionospheric current system. The main objective of this paper is to evaluate the significance of one of those typically ignored processes, namely neutral-wind-driven currents, on GMDs.

Neutral wind dynamo is an essential part of the overall electrodynamics in the ionosphere and thermosphere (IT) system as reported by various papers [e.g., *Blanc and Richmond*, 1980; *Thayer and Vickrey, 1992*; *Deng et al.*, 1993; *Lu et al.*, 1995]. At low and middle latitudes, ionospheric currents are mainly driven by the polarization electric fields generated by the neutral wind dynamo and can be impacted by the magnetosphere forcing through penetration electric field (PEF) during geomagnetically active times. At high latitudes, although the magnetospheric convection electric

This article is protected by copyright. All rights reserved.

Author Manuscript

fields are the primary drivers for ionospheric currents, the neutral wind dynamo contribution is not negligible. A modeling study of the March 28-29, 1992 event by *Lu et al.* [1995] showed that the hemispheric integral of the total field-aligned currents (FACs) driven by the neutral winds is about 27% of the total FACs driven by the magnetosphere convection on average. In addition, the neutral-wind-driven FACs are found to flow in the opposition direction as those driven by the magnetosphere convection. Using coupled magnetosphere-ionosphere-thermosphere models, *Ridley et al.* [2003] and *Wang et al.* [2007] also found similar conclusions regarding the significance of neutral-wind-driven FACs.

An interesting phenomena about the neutral-wind-driven currents is the "flywheel" effect, which refers to the neutral-wind-driven currents during the recovery phase of geomagnetic storms [*Banks*, 1972; *Lyons et al.*, 1985; *Deng et al.*, 1993]. In response to the high-latitude momentum and energy inputs, the thermosphere wind response is generally characterized by enhanced upwelling and horizontal winds at high latitudes and a global wind surge propagating from high to middle and low latitudes [*Fuller-Rowell et al.*, 1994; 2008; *Emmert et al.*, 2002; *Joshi et al.*, 2015]. During the recovery phase when the magnetosphere forcing is weakened, it takes a long period of time for neutral winds to recover and return to the quiet-time state due to the large inertia of the neutrals. Therefore, neutrals may have a larger speed than ions and drive a significant current system. Simulation studies conducted in *Deng et al. [1991]* suggested that neutral winds might drive as much as 80% of the high-latitude current system (both horizontal ionospheric currents and FACs) immediately after a storm has ended and might continue to dominate the current system for 4 to 5 hours. *Wang et al.* [2007] argued that the magnitude of neutral-wind-driven currents depends on the magnitudes of both neutral winds and ionospheric conductivity and demonstrated that the mismatch between the peak altitudes of the ionospheric conductivity and the storm enhanced

This article is protected by copyright. All rights reserved.

Author Manuscript

neutral winds limits the development of neutral-wind-driven currents. In their event study, the total (area integration above 45° geomagnetic latitudes) neutral-wind-driven FACs are about 20% and 27% of those due to the magnetosphere convection during the main and recovery phase, respectively. The relative importance of neutral-wind-driven currents does not show strong dependence on the storm phase. However, as shown in *Wang et al.* [2007], most previous studies focus on the neutral-wind-driven currents and their relative importance at high latitudes where the currents maximize, or the hemispheric integrated currents which are mostly contributed by the high-latitude component. The significance of the neutral-wind-driven currents at middle latitudes is not clear, especially during the storm recovery phase. It is still an open question how these neutral-wind-driven currents at middle latitudes would affect GMDs and therefore GICs.

This paper presents a different approach than using MHD models to estimate GMDs by using a 3-dimensional ionosphere and thermosphere general circulation model (GCM), which describes the ionosphere-thermosphere (IT) system in a self-consistent way. Our methodology is described in Section 2. Simulations of an idealized storm event have been conducted and the relative significance of neutral-wind-driven currents on GMDs has been evaluated for different storm phases and at different latitudes as shown in Section 3.

2. Methodology

GITM is a three-dimensional GCM for the coupled IT system [*Ridley et al.*, 2006]. It solves the continuity, momentum, and energy equations for the neutrals and ions self-consistently in an altitude-based grid. The model calculates the neutral density, neutral winds, and temperature as well as ion density, velocity, and temperature. The model does not assume a hydrostatic equilibrium for the neutrals in the vertical direction, which enables the investigations of non-hydrostatic effects in the upper atmosphere [*Deng et al.*, 2008, 2011; *Deng and Ridley*, 2014].

This article is protected by copyright. All rights reserved.

Author Manuscript

Meanwhile, the number of grid points in each direction can be specified and therefore the resolution is flexible. In this study, the model has been run with a resolution of 2.0° in geographic latitude (GLat), 5.0° in geographic longitude (GLon), and 1/3 scale height in the vertical direction (~1.5 km at an altitude of 100 km and ~15.0 km at an altitude of 300 km, 50 grid points in total). The high-latitude electric potential is specified by the *Weimer* [2005] model, and the auroral electron precipitation is specified by the *Fuller-Rowell and Evans* [1987] model.

$$\vec{J}_{Horizontal} = \sigma_P\left(\vec{E} + \vec{U} \times \vec{B}\right) + \sigma_H \hat{b} \times \left(\vec{E} + \vec{U} \times \vec{B}\right) \quad (1)$$

$$\vec{J}_{\parallel} = -\frac{1}{\sin I}\int_{z_1}^{z_2} \nabla \cdot \left[\sigma_P\left(\vec{E} + \vec{U} \times \vec{B}\right) + \sigma_H \hat{b} \times \left(\vec{E} + \vec{U} \times \vec{B}\right)\right] dz \quad (2)$$

In GITM simulations, the horizontal ionospheric currents ($\vec{J}_{Horizontal}$) are calculated using Equation (1), in which σ_P is Pedersen conductivity, $\sigma_H$is Hall conductivity, $\vec{U}$ is neutral wind, $\vec{B}$ is the magnetic field, and $\hat{b}$ is the unit vector of the magnetic field. A pure dipole field has been used to represent the Earth's magnetic field. The magnetospheric convection electric field is represented by $\vec{E}$, and neutral-wind-driven electric field is represented by $\vec{U} \times \vec{B}$. Following *Lu et al.* [1995], FACs ($\vec{J}_{\parallel}$) can be estimated using Equation (2), in which I is the downward inclination angle of $\vec{B}$, z is altitude, and $z_1$and z_2 are the bottom and top of the IT system. Positive $\vec{J}_{\parallel}$ means that it flows out of the ionosphere. GMDs are calculated using the Biot-Savart law with horizontal ionospheric currents from Equation (1) and FACs from Equation (2) as the current sources. Currents and GMDs are calculated at each time step of the simulation. In this study, simulation outputs are saved every five seconds.

3. Results

3.1 FACs and GMDs at Different Phases of an Idealized Event

This article is protected by copyright. All rights reserved.

Author Manuscript

From top to bottom, Figure 1 shows the temporal variation of the interplanetary magnetic field (IMF) B_y and B_z, solar wind speed, solar wind pressure, and hemispheric power for precipitating electrons during an idealized event. The hemispheric power is estimated based on the IMF and solar wind conditions [*Codrescu et al.*, 2012]. The simulation period starts at 00 UT and last for five hours, with one-hour quiet time, three-hour active time, and one-hour recovery time. IMF and solar wind conditions are kept as constant during each phase of the idealized event, and step functions are used when transitioning from one phase to another. During the quiet time, IMF B_y is 0 nT, IMF B_z is -1 nT, solar wind speed is 400 km/s, solar wind pressure is 1 nPa, and the estimated hemispheric power is 15 GW. During the active time, IMF B_y stays at 0 nT, IMF B_z changes to -20 nT, solar wind speed increases to 800.0 km/s, solar wind pressure changes to 5 nPa, and the estimated hemispheric power becomes 93.5 GW correspondingly. IMF and solar wind conditions during the recovery time are the same as those during the quiet time. GITM simulations of this idealized event are conducted under equinox conditions with a F10.7 of 150.0 solar flux units (sfu).

IMF and solar wind conditions in Figure 1 are used to drive the *Weimer* [2005] model, which specifies the high-latitude electric potential in GITM. Hemispheric power is used as an input to the *Fuller-Rowell and Evans* [1987] model, which specifies the auroral electron precipitation. Figure 2 shows some snapshots of the high-latitude electric potential (top row) and electron energy flux (bottom row) during the quiet (left column, at 00:30:00 UT), active (middle column, at 02:30:00 UT), and recovery (right column, at 05:00:00 UT) times in geographic coordinates. The outer ring in each plot is 40°N. Cross polar cap potential (CPCP) is shown in the top left corner of panels (a), (b), and (c), and hemispheric-integrated electron energy flux is shown in the top left corner of panels (d), (e), and (f). From the quiet to the active time, the low-latitude boundary of the electric potential pattern expands from about ~60°N to ~45°N, and CPCP increases from 46.1

This article is protected by copyright. All rights reserved.

Author Manuscript

to 220.4 kV. Meanwhile, the maximum electron energy flux increases from 2.16 to 13.16 mW/m^2 and the hemispheric-integrated electron energy flux increases from 21.1 to 136.3 GW. Substantial ionospheric and thermospheric disturbances and intensified ionospheric currents are expected given such strong IMF and solar wind conditions during the active time.

Distributions of FACs in geographic coordinates, which are calculated using Equation (2), due to different sources and at different phases of the idealized event are shown in Figure 3 and are used to evaluate the significance of neutral-wind-driven currents. The top, middle, and bottom rows show the distributions of FACs during the quiet, active, and recovery times, respectively. The left, middle, and right columns show the distributions of the total FACs, FACs due to magnetospheric convection (the terms related to $\vec{E}$ in Equation (2)), and neutral-wind-driven FACs (the terms related to $\vec{U} \times \vec{B}$ in Equation (2)), respectively. To better display the features of FACs at all latitudes, the color bar ranges have been set as $\pm 1.0\ \mu A/m^2$ for the quiet and recovery times, and $\pm 2.0\ \mu A/m^2$ for the active time, respectively. From the quiet (top) to the active (middle) time, distributions of FACs due to both magnetospheric convection and neutral winds expand from high to middle latitudes, and the maximum magnitude is more than doubled. From the active (middle) to the recovery time, FACs due to magnetospheric convection return to the quiet-time state since the IMF and solar wind drivers are the same during the quiet and recovery times. However, FACs due to neutral winds display very different variations. As shown in Figure 3i, on the nightside, neutral-wind-driven FACs contract to ~60^{0}N, which is close to the equatorward boundary of the FACs due to the magnetospheric convection. On the dayside, neutral-wind-driven FACs persist at all latitudes and all local times, and their magnitudes are comparable to those driven by the magnetospheric convection during the recovery time (Figure 3h). The mechanisms generating these dayside FACs are discussed in the next section. At locations where the high-latitude electric

This article is protected by copyright. All rights reserved.

Author Manuscript

potential is dominant, neutral-wind-driven FACs are secondary compared to those driven by the magnetospheric convection during all phases of the idealized event and at all latitudes. The magnitude of neutral-wind-driven FACs is about 10-30% of the total FACs, depending on the location. Neutral-wind-driven FACs often flow in the opposite directions as those driven by magnetospheric convection. Overall, our results are consistent with previous studies [*Lu et al.*, 1995; *Ridley et al.*, 2003; *Wang et al.*, 2007]. Neutral winds impact both horizontal ionospheric currents and FACs, which are strongly correlated with each other through the current continuity equation. In addition to FACs, the height-integrated horizontal ionospheric currents have also been examined (Figures S2 and S3), and the neutral wind contribution to horizontal ionospheric currents is in the similar range as that to FACs (10-30%).

Distributions of GMDs in the meridional direction (geographic coordinates, positive for northward) are shown in Figure 4 and are organized in the same way as in Figure 3. The color bar ranges have been set as $\pm 110.0\ nT$ for the quiet and recovery times, and $\pm 1100.0\ nT$ for the active time, respectively. The variation of GMDs follows a very similar trend as FACs such as (1) the distribution expands equatorward with enhanced magnitudes during the active time; (2) the distribution of GMDs due to magnetospheric convection retreats to high latitudes from the active to the recovery time. The relative significance of neutral-wind-driven GMDs is also very similar to that of neutral-wind-driven FACs. At locations where the high-latitude electric potential is dominant, neutral-wind-driven GMDs are secondary compared to those driven by magnetospheric convection, contributing to about 10-30% of the total GMDs. During the recovery phase, neutral-wind-driven GMDs are also found to exist with notable magnitudes on the dayside and at middle latitudes, where the magnetospheric convection electric field is absent. GMDs in the zonal and vertical directions have also been examined, and distributions of GMDs in the zonal direction have

This article is protected by copyright. All rights reserved.

Author Manuscript

been shown in Figure S1. They display very similar variations as GMDs in the meridional direction, and similar conclusions can be drawn. Our results suggest that neutral-wind-driven GMDs are not negligible and that the neutral wind dynamo could be an important source for GMDs at middle latitudes during the recovery phase. Therefore, neutral wind effects should be considered when calculating ionospheric currents and GMDs.

3.2 "Flywheel" Currents and Their Impact on GMDs at Middle Latitudes

As discussed in Section 3.1, one of our major findings is that neutral-wind-driven currents and GMDs with notable magnitudes exist at middle latitudes during the recovery phase. Since our simulation does not include a ring current model component, ring currents and their impact on GMDs are not considered in our analysis due to the limitation of our methodology. As a result, neutral winds become the sole driver of ionospheric currents (Figure 3g vs. Figure 3i) and GMDs (Figure 4g vs. Figure 4i) at middle latitudes during the recovery phase. The driving mechanism of these dayside currents and GMDs is the flywheel effect as discussed in many previous studies [*Banks*, 1972; *Lyons et al.*, 1985; *Deng et al.*, 1993], which can be attributed to the long recovery of neutral winds from active times.

In Figure 5, the left column shows the meridional wind at 110 km during different phases of the event, and the right column shows the corresponding height-integrated horizontal ionospheric currents in the zonal direction (geographic coordinates). From the quiet to the active time, disturbed meridional winds with larger magnitudes are found at both high and middle latitudes on both dayside and nightside. Correspondingly, the height-integrated horizontal current expands to middle latitudes and its maximum magnitude is ~4 times larger than the quiet-time value. From the active to the recovery time, meridional winds have not returned to the quiet-time state yet due to the relatively large inertial of neutrals and storm enhanced winds can still be found across

This article is protected by copyright. All rights reserved.

Author Manuscript

different latitudes on both dayside and nightside. *Wang et al.* [2007] pointed out that the development of neutral-wind-driven currents requires both enhanced neutral winds and large ionospheric conductivity. Indeed, during the recovery phase, neutral-wind-driven currents (both horizontal and radial) and therefore GMDs are most significant (1) at auroral latitudes on the nightside, where large ionospheric conductivity is produced by auroral electron precipitation; and (2) across different latitudes on the dayside, where large ionospheric conductivity is produced by solar radiation.

3.3 Latitudinal dependence of GMDs

To illustrate the relative significance of neutral-wind-driven GMDs at different latitudes, GMDs in the meridional direction at two selected locations, [70°N, 120°E] and [55°N, 120°E], are plotted out in Figure 6. At 120°E, the local time is 08:00 at 00:00 UT (the start of the event) and 13:00 at 05:00 UT (the end of the event). At [70°N, 120°E], GMDs due to neutral winds (blue line) have the opposite sign of those due to magnetospheric convection (red line) during the active time when the high-latitude electric potential is dominant, and GMDs due to neutral winds are about 10-30% of those due to the magnetospheric convection. During the recovery phase, magnetospheric convection is weakened, and GMDs due to magnetospheric convection drops substantially. However, neutral winds take longer time to recover and GMDs due to neutral winds have a larger magnitude than those due to magnetospheric convection in the recovery phase at this location. The flywheel effect is more profound at the middle-latitude location ([55°N, 120°E]). During the active phase, GMDs are primarily contributed by magnetospheric convection. The sign change of GMDs from negative to positive around 0205 UT is due to the local time dependence as shown in Figure 4. During the recovery phase, magnetospheric convection retreats to higher latitudes and is absent at this location, and therefore, GMDs are solely contributed by neutral wind-induced currents. The

This article is protected by copyright. All rights reserved.

Author Manuscript

magnitude of the recovery-time neutral-wind-driven GMDs is about 50 nT at this location, which is comparable to that caused by ring currents at middle latitudes during storm recovery phases [*Welling et al.*, 2019].

This paper presents simulation results for an idealized event, in which the IMF and solar wind conditions are kept constant during each phase. Therefore, GMDs do not show too many temporal variations. During real events, both observations and simulations show that GMDs have strong temporal and spatial variations at different scales [e.g., *Pulkkinen et al.*, 2013; *Welling et al.*, 2021]. In future study, GITM simulations will be conducted for real geomagnetic storm events, and simulated GMDs and dB/dt will be compared with ground magnetometer measurements to further evaluate the importance of neutral-wind-driven ionospheric currents. Nevertheless, our results suggest that in real events, neutral winds may be one important source for GMDs and may subsequently contribute to GICs at middle latitudes during the recovery phase.

5. Summary

This paper presents an approach to estimate GMDs by using an ionosphere and thermosphere general circulation model, other than MHD models. Specifically, GITM simulations have been carried out for an idealized event and the significance of neutral-wind-driven currents and GMDs have been evaluated at different phases of the event. At locations where the high-latitude electric potential is dominant, FACs due to neutral winds are found to be about 10-30% of the total FACs. At middle latitudes, especially on the dayside, the neutral-wind-driven currents and GMDs with notable magnitudes exist during the recovery phase due to the flywheel effect. Since the magnetosphere convection retreats to higher latitudes and is absent at middle latitudes during the recovery phase, ionospheric currents and GMDs are solely driven by neutral winds at these locations in our simulations. The magnitude of neutral-wind-driven GMDs at middle latitudes

This article is protected by copyright. All rights reserved.

Author Manuscript

during the recovery phase is about a few tens of nT, which is comparable to that caused by ring currents in the same latitudinal range. Our results suggest that neutral wind effects should not be ignored in estimating FACs, GMDs, and subsequent impacts (such as GICs), especially at middle latitudes.

Acknowledgments

This work at UTA was supported by NASA through grants 80NSSC20K1786, 80NSSC22K0061, 80NSSC20K0195 and 80GSFC22CA011, and AFOSR through award FA9559-16-1-0364. Dr. Welling's contributions were funded via the Solar Tsunami project from the University of Otago and the New Zealand Ministry of Business, Innovation, and Employment as well as NSF grant AGS2305408. The work at LANL was supported by 80HQTR21T0003. We thank the support from ISSI for the international team on "Multi-Scale Magnetosphere-Ionosphere-Thermosphere Interaction". The authors acknowledge the Texas Advanced Computing Center (TACC, http://www.tacc.utexas.edu) at the University of Texas at Austin for providing HPC resources that have contributed to the research results reported within this paper.

Open Research

Model simulations for this study were conducted on TACC supercomputers. Model outputs are saved in binary format and are available at *Sheng et al.* [2023].

This article is protected by copyright. All rights reserved.

Author Manuscript

Author Manuscript

References

Banks, P. M. (1972, January). Magnetospheric processes and the behavior of the neutral atmosphere. In Plenary Meeting on Space research XII.

Blanc, M., & Richmond, A. D. (1980). The ionospheric disturbance dynamo. Journal of Geophysical Research: Space Physics, 85(A4), 1669-1686.

Boteler, D. H. (2001). Assessment of geomagnetic hazard to power systems in Canada. Natural Hazards, 23, 101-120.

Codrescu, M. V., Negrea, C., Fedrizzi, M., Fuller-Rowell, T. J., Dobin, A., Jakowsky, N., ... & Maruyama, N. (2012). A real-time run of the Coupled Thermosphere Ionosphere Plasmasphere Electrodynamics (CTIPe) model. *Space Weather, 10*(2).

Deng, W., Killeen, T. L., Burns, A. G., & Roble, R. G. (1991). The flywheel effect: Ionospheric currents after a geomagnetic storm. Geophysical research letters, 18(10), 1845-1848.

Deng, W., Killeen, T. L., Burns, A. G., Roble, R. G., Slavin, J. A., & Wharton, L. E. (1993). The effects of neutral inertia on ionospheric currents in the high-latitude thermosphere following a geomagnetic storm. Journal of Geophysical Research: Space Physics, 98(A5), 7775-7790.

Deng, Y., Richmond, A. D., Ridley, A. J., & Liu, H. L. (2008). Assessment of the non-hydrostatic effect on the upper atmosphere using a general circulation model (GCM). *Geophysical Research Letters, 35*(1).

Deng, Y., Fuller-Rowell, T. J., Akmaev, R. A., & Ridley, A. J. (2011). Impact of the altitudinal Joule heating distribution on the thermosphere. *Journal of Geophysical Research: Space Physics, 116*(A5).

Deng, Y., & Ridley, A. J. (2014). Simulation of non-hydrostatic gravity wave propagation in the upper atmosphere. *Ann. Geophys, 32*(4), 443-447.

Emmert, J. T., Fejer, B. G., Shepherd, G. G., & Solheim, B. H. (2002). Altitude dependence of middle and low-latitude daytime thermospheric disturbance winds measured by WINDII. Journal of Geophysical Research: Space Physics, 107(A12), SIA-19.

Fuller-Rowell, T. J., Codrescu, M. V., Moffett, R. J., & Quegan, S. (1994). Response of the thermosphere and ionosphere to geomagnetic storms. Journal of Geophysical Research: Space Physics, 99(A3), 3893-3914.

Fuller-Rowell, T. J., & Evans, D. S. (1987). Height-integrated Pedersen and Hall conductivity patterns inferred from the TIROS-NOAA satellite data. *Journal of Geophysical Research: Space Physics, 92*(A7), 7606-7618.

Fuller-Rowell, T. J., Richmond, A. D., & Maruyama, N. (2008). Global modeling of storm-time thermospheric dynamics and electrodynamics. Washington DC American Geophysical Union Geophysical Monograph Series, 181, 187-200.

Gummow, R. A., & Eng, P. (2002). GIC effects on pipeline corrosion and corrosion control systems. Journal of Atmospheric and Solar-Terrestrial Physics, 64(16), 1755-1764.

Joshi, P. P., H. Baker, J. B., Ruohoniemi, J. M., Makela, J. J., Fisher, D. J., Harding, B. J., ... & Thomas, E. G. (2015). Observations of storm time midlatitude ion-neutral coupling using

This article is protected by copyright. All rights reserved.

Author Manuscript

SuperDARN radars and NATION Fabry-Perot interferometers. Journal of Geophysical Research: Space Physics, 120(10), 8989-9003.

Lu, G., Richmond, A. D., Emery, B. A., & Roble, R. G. (1995). Magnetosphere-ionosphere-thermosphere coupling: Effect of neutral winds on energy transfer and field-aligned current. Journal of Geophysical Research: Space Physics, 100(A10), 19643-19659.

Lyons, L. R., Killeen, T. L., & Walterscheid, R. L. (1985). The neutral wind "flywheel" as a source of quiet-time, polar-cap currents. Geophysical research letters, 12(2), 101-104.

Ngwira, C. M., & Pulkkinen, A. A. (2019). An introduction to geomagnetically induced currents. Geomagnetically induced currents from the sun to the power grid, 1-13.

Ridley, A. J., Richmond, A. D., Gombosi, T. I., De Zeeuw, D. L., & Clauer, C. R. (2003). Ionospheric control of the magnetospheric configuration: Thermospheric neutral winds. Journal of Geophysical Research: Space Physics, 108(A8).

Ridley, A. J., Deng, Y., & Toth, G. (2006). The global ionosphere–thermosphere model. *J. Atmos. Sol. Terr. Phys., 68*(8), 839-864.

Robinson, R. M., Vondrak, R. R., Miller, K., Dabbs, T., & Hardy, D. (1987). On calculating ionospheric conductances from the flux and energy of precipitating electrons. Journal of Geophysical Research: Space Physics, 92(A3), 2565-2569.

Sheng, C., Deng, Y., Welling, D. T., & Morley, S. K. (2023). Ground Magnetic Disturbances due to Neutral-wind-driven Ionospheric Currents [Data set]. Zenodo. https://doi.org/10.5281/zenodo.8403787.

Thayer, J. P., & Vickrey, J. F. (1992). On the contribution of the thermospheric neutral wind to high-latitude energetics. Geophysical research letters, 19(3), 265-268.

Wang, W., Burns, A. G., Wiltberger, M., Solomon, S. C., & Killeen, T. L. (2007). An analysis of neutral wind generated currents during geomagnetic storms. Journal of atmospheric and solar-terrestrial physics, 69(1-2), 159-165.

Weimer, D. R. (2005). Improved ionospheric electrodynamic models and application to calculating Joule heating rates. *Journal of Geophysical Research: Space Physics, 110*(A5).

Welling, D. T., Anderson, B. J., Crowley, G., Pulkkinen, A. A., & Rastätter, L. (2017). Exploring predictive performance: A reanalysis of the geospace model transition challenge. *Space Weather, 15*(1), 192-203.

Welling, D. (2019). Magnetohydrodynamic models of B and their use in GIC estimates. Geomagnetically induced currents from the sun to the power grid, 43-65.

Welling, D. T., Love, J. J., Rigler, E. J., Oliveira, D. M., Komar, C. M., & Morley, S. K. (2021). Numerical simulations of the geospace response to the arrival of an idealized perfect interplanetary coronal mass ejection. Space weather, 19(2), e2020SW002489

This article is protected by copyright. All rights reserved.

Author Manuscript

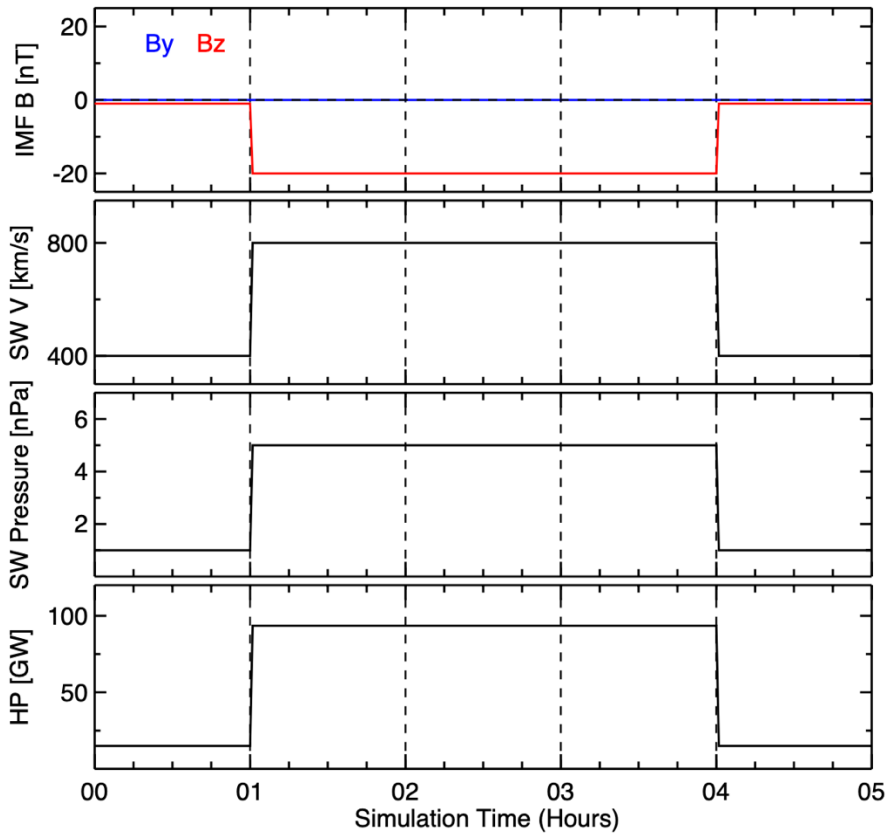


Figure 1. IMF and solar wind conditions of an idealized event. From top to bottom: IMF B_y and B_z (nT), solar wind speed (km/s), solar wind pressure (nPa), and hemispheric power (GW) estimated from IMF and solar wind conditions.

This article is protected by copyright. All rights reserved.

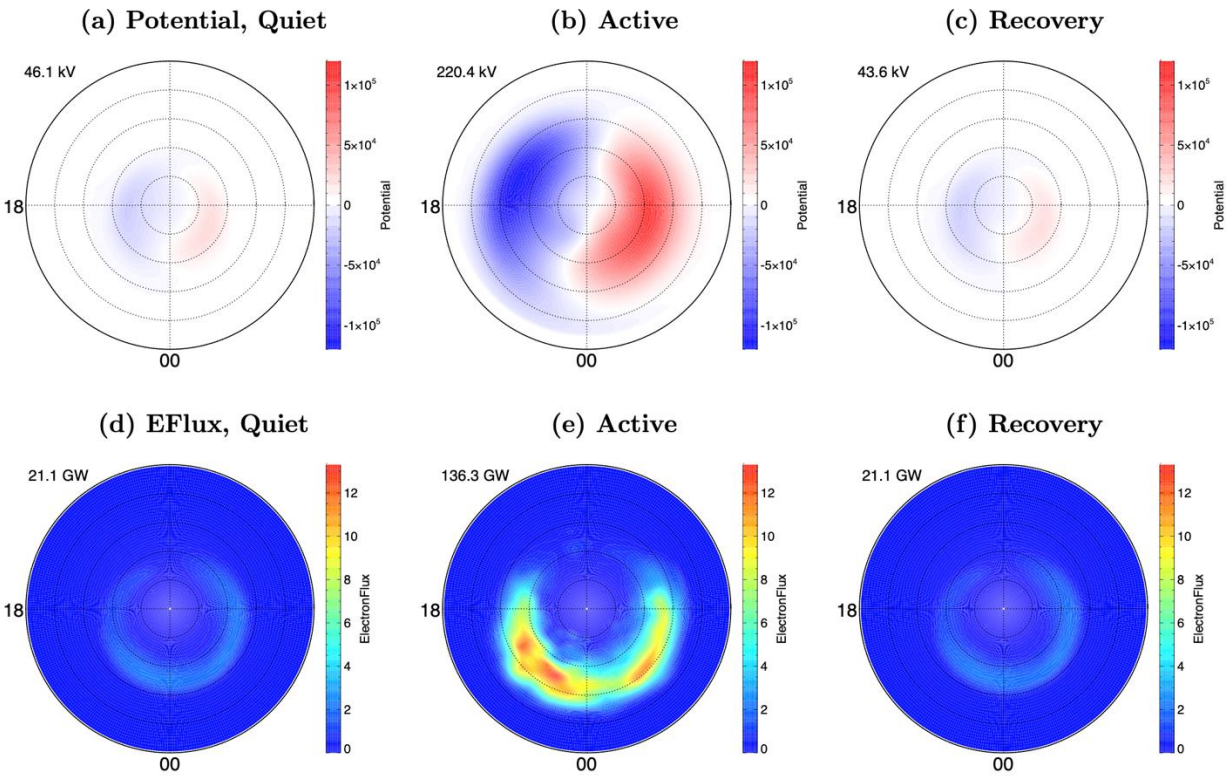


Figure 2. High-latitude electric potential (in V, top, specified by the *Weimer* [2005] model) and auroral electron energy flux (in mW/m^2, bottom, specified by the *Fuller-Rowell and Evans* [1987] model) during the quiet (left, 00:30 UT), active (middle, 02:30 UT), and recovery (right, 05:00 UT) times of the idealized event in geographic coordinates. The outer ring is 40°N for all the polar plots in this paper.

Author Manuscript

This article is protected by copyright. All rights reserved.

Author Manuscript

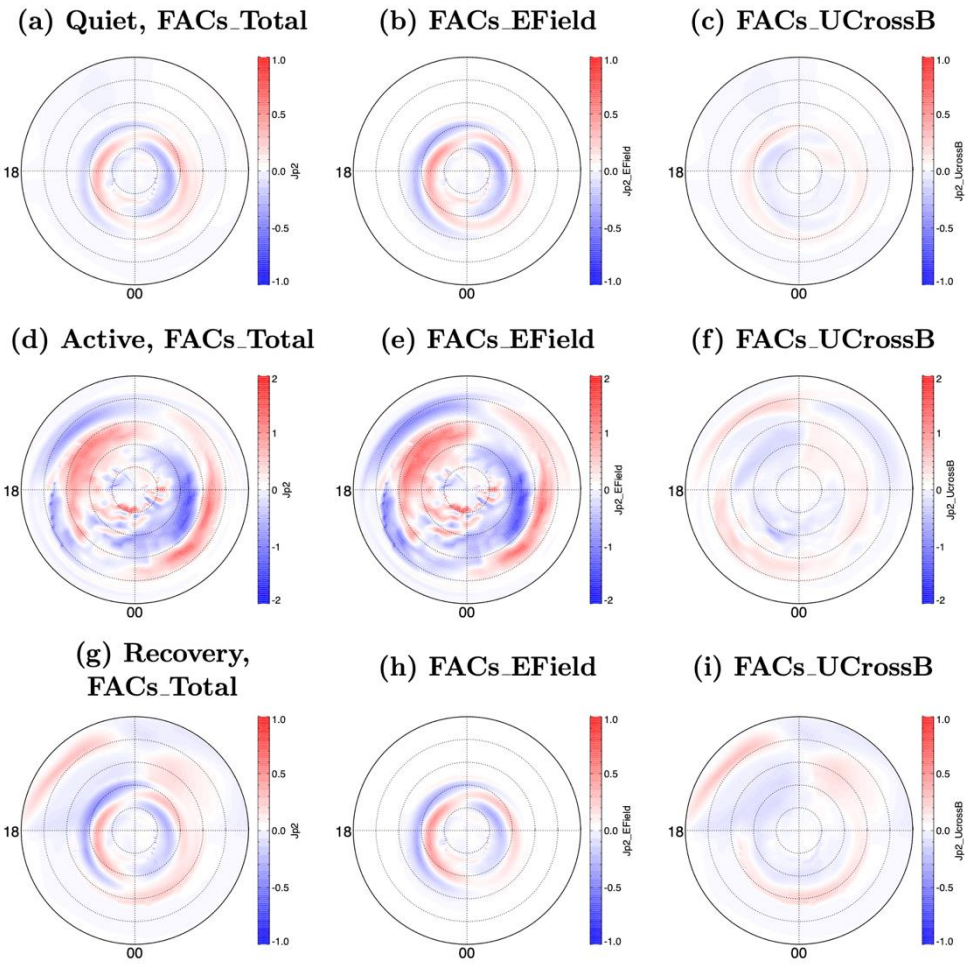


Figure 3. Distributions of the total FACs (left column), FACs due to magnetosphere convection (middle column), and neutral-wind-driven FACs (right column) during the quiet (top row), active (middle row), and recovery times (bottom row) in geographic coordinates. The color bar ranges have been set as ±1.0 $\mu A/m^2$ for the quiet and recovery times and ±2.0 $\mu A/m^2$ for the active time, respectively.

This article is protected by copyright. All rights reserved.

Author Manuscript

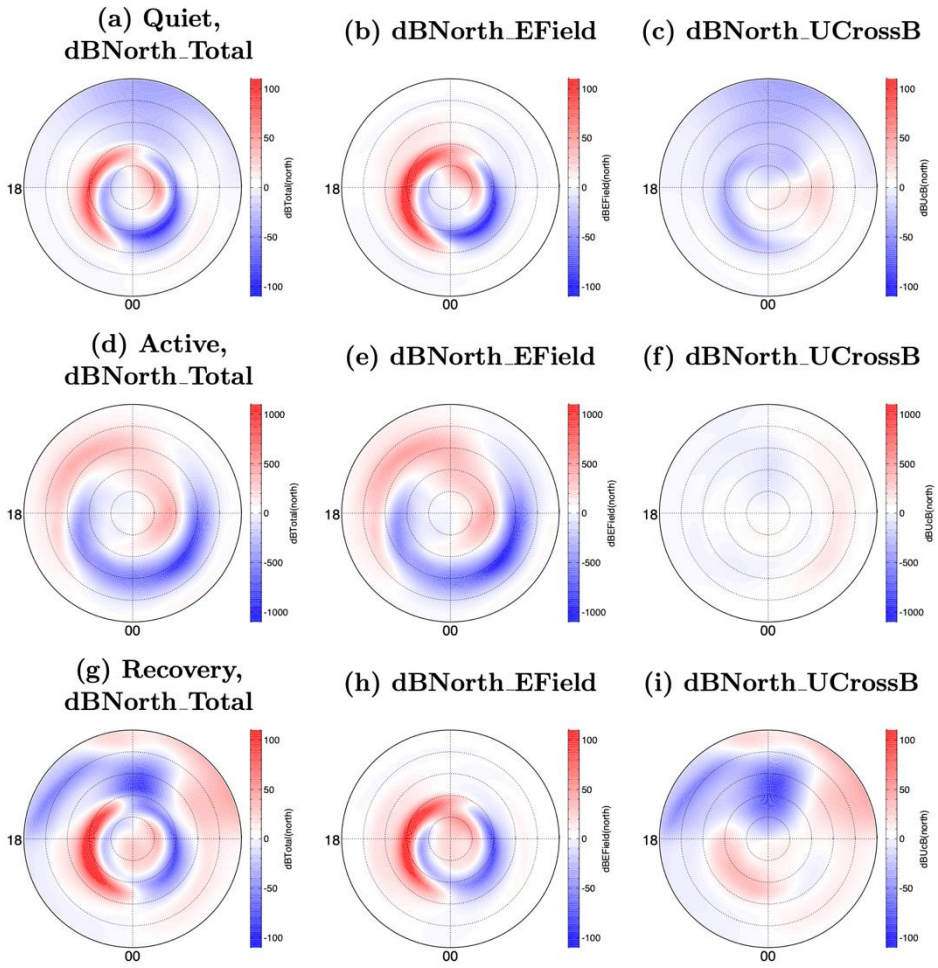


Figure 4. Same as Figure 3 but for GMDs. The color bar ranges have been set as ±110.0 nT for the quiet and recovery times and ±1100.0 nT for the active time, respectively.

This article is protected by copyright. All rights reserved.

Author Manuscript

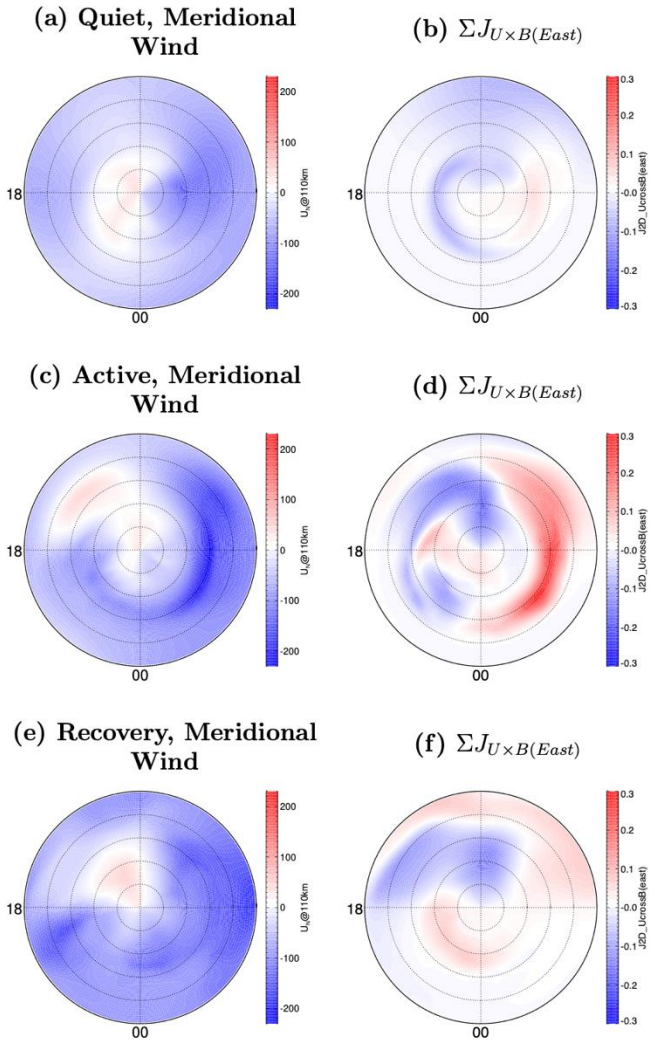


Figure 5. Zonal winds at 110 km (in m/s, left) and height-integrated horizontal ionospheric currents in the meridional direction (in A/m, geographic coordinates) during the quiet (top row), active (middle row), and the recovery (bottom row) times in geographic coordinates.

This article is protected by copyright. All rights reserved.

Author Manuscript

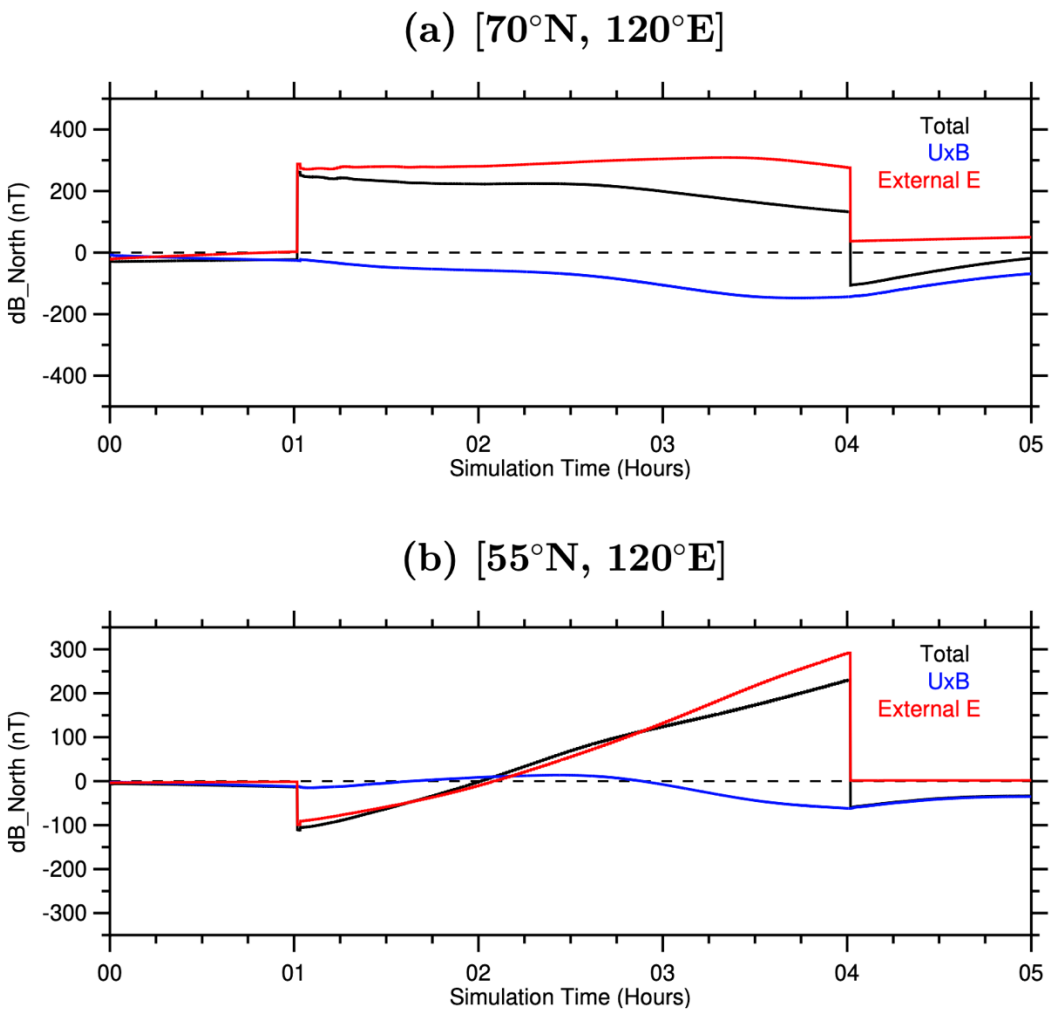


Figure 6. GMDs in the meridional direction (geographic coordinates) at [70°N, 120°E] (a) and [55°N, 120°E] (b) from 00:00 to 05:00 simulation hours. The simulation starts at 00:00 UT. The black, red, and blue lines depict the total GMDs, GMDs due to magnetosphere convection, and GMDs due to neutral winds, respectively.

This article is protected by copyright. All rights reserved.